SOILS AND FOUNDATIONS Vol. 12, No. 4, Dec. 1972
Japanese Society of Soil Mechanics and Foundation Engineering

DEFORMATION MECHANISM OF SAND IN TRIAXIAL COMPRESSION TESTS

MASANOBU ODA*

ABSTRACT

Based on detailed observations by using a microscope and thin section method, a new granular model has been proposed as a basis of theoretical considerations on granular mechanics.

The specimen deformed to residual stress state can be divided into three subdomains having each homogeneous fabric, i.e., dead domain, dilated domain and shear domain. The void ratio in the dilated domain becomes equal to 20% relative density at peak stress state whose value represents an unstable particle configuration in a granular material. Concentration of directions (N_i) perpendicular to tangential planes at contacts to the maximum principal stress direction performs an essential role in strengthening granular fabric up to the peak stress state. Relative movements between particles in the shear domain occur principally by preferred sliding along the contacts having N_i inclined to σ_1-direction about 35°, and partially by rolling of each grain to reorient preferred dimensional orientation. Mobilized stress ratio of granular materials when subjected to a deviatoric stress state is found to depend not only upon the interparticle friction angle between grains ϕ_μ but also upon the parameter representing fabric anisotropy S_z/S_x. Experiments on two kinds of sand show that theoretical equation is closely obeyed by experimental results throughout deformation to failure irrespective of their initial void ratio and initial fabric.

Key words: dilatancy, microscopy, failure, progressive failure, residual strength, sand, soil structure, drained triaxial compression test

IGC: D6/D3

INTRODUCTION

Non-elastic deformation of granular material as sand is usually considered to occur due to frictional slidings between its constituting grain particles. When we intend to obtain theoretical equations concerning its mechanical behaviour, it is essential to have confirmed knowledges of the following important problems;

(1) the mechanical role of sliding and rolling of grains during deformation,
(2) the mechanism to form a shear plane or shear zone in granular fabric,
(3) the mechanism to control fabric reconstruction, and
(4) the proper assessment of peculiar mechanical behaviour of granular material such as dilatancy and critical void ratio.

Although several interesting papers have been published on these problems (Newland and

* Assistant, Department of Foundation Engineering, Faculty of Science and Engineering, University of Saitama, Urawa, Saitama.
Written discussions on this paper should be submitted before October 1, 1973.

Allely, 1957; Roscoe, 1958; Rowe, 1962; Rowe, 1963; Rowe, 1964; Murayama, 1964; Horne, 1965; Horne, 1969; Mogami, 1965; Mogami, 1966; Murayama and Matsuoka, 1970; Wilkins, 1970; Ingles, et al, 1971), it seems to the present writer that none of the granular models introduced by these authors have been supported by the confirmed knowledge of the deformation mechanism of microscopic scale.

In this paper the above-mentioned problems will be discussed in detail and the most reliable granular model will be proposed as a basis of theoretical considerations of granular mechanics.

TESTING MATERIAL AND TESTING PROCEDURES

Granular material used in this study is a uniform sand (0.59~0.84 mm) which is composed of 90% quartz and 10% feldspar. The index properties of the sand are shown in Table 1.

Table 1. Index properties of sand

Specific gravity	Limiting void ratio		Axial ratio	Roundness
	Maximum	Minimum		
2.65	0.96	0.61	0.67	Subround to subangular

The experiment consists of three series as follows:

(1) P-series: Sand is compacted by the plunging method (Oda, 1972b) to prepare specimens whose initial void ratio (e_0) is equal to 0.71.

(2) T-series: Sand is compacted by the tapping method to prepare specimens whose initial void ratio is equal to that of P-series.

(3) L-series: Specimens are made by placing grains in a split mold with a spoon as loose as possible (e_0=0.83).

Drained triaxial compression tests on these specimens are carried out by using a conventional triaxial soil testing machine at constant confining pressure (1.0 kg/cm^2) at constant strain rate (0.3%/min). The average stress-strain-volumetric strain curves for the three series of experiments of sand are shown in Fig. 1. In this figure the positions at which specific tests were terminated are indicated. Final axial strain, stress ratio, deformation modulus, initial void ratio, and so on are represented in Table 2.

In order to observe the granular fabric of these specimens by the microscope and thin section method, the deformed and undeformed specimens are fixed without disturbing the relative configuration relation of sand particles by means of the previously described method (Oda, 1972b). These fixed specimens are cut with a diamond saw along two vertical planes and a horizontal plane. Thin sections prepared parallel to these planes are called tentatively V-section and H-section, respectively.

Reference axes X, Y and Z are defined as follows: X-axis is an intersection of the horizontal and the vertical planes (if a shear plane can be seen with the naked eyes in the deformed specimen, the intersection of the horizontal plane and the shear plane is selected as X-axis), Z-axis is the vertical direction which coincides with the direction of compression, and Y-axis is perpendicular to X- and Z-axes.

FABRIC ANALYSES AND THEIR RESULTS

Concept of homogeneous fabric of granular mass should include at least two main sub-

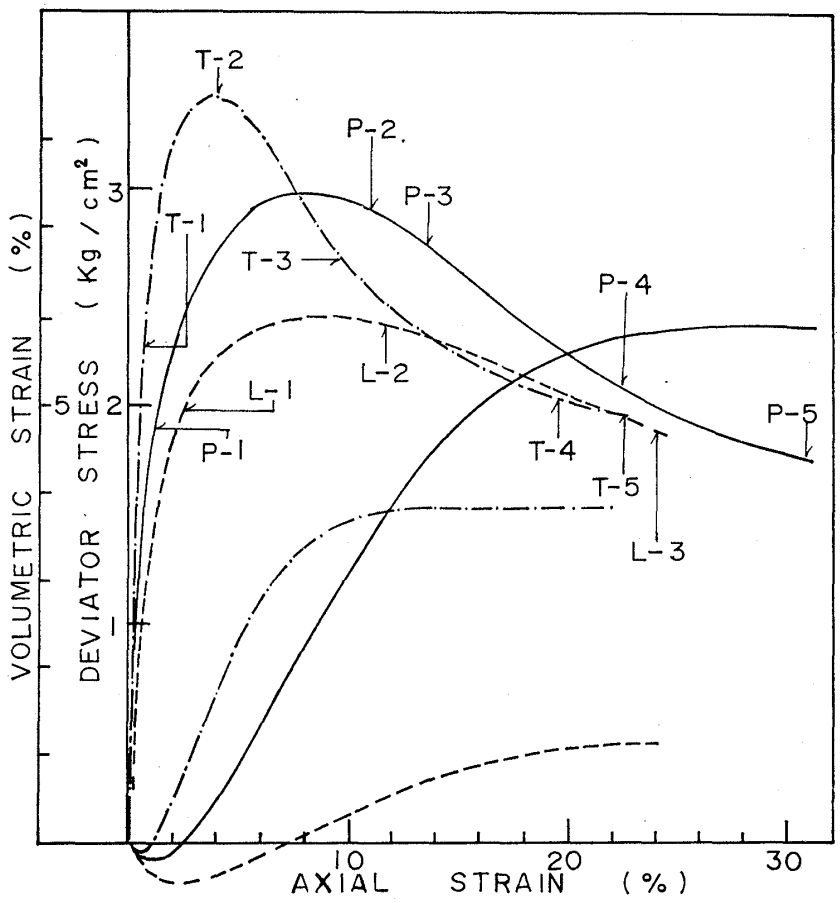

Fig. 1. Stress-strain-volumetric strain curves for the three series of experiments of sand

concepts, i.e., (1) orientation of an individual particle, and (2) position of a particle and its mutual relationship to other particles. The orientation of particles can be successfully estimated by the determination of degree of preferred orientation or parallelism of apparent longest axes observed in the V-section (Lafeber, 1966; Oda, 1972a). The mutual relation of particles to other particles is represented by the three-dimensional probability density function $E(\alpha, \beta)$ of directions (N_i) normal to tangential planes at contacts, where α and β are spherical coordinates to define the direction N_i with respect to the reference axes as shown in Fig. 6 (Oda, 1972a and b), and by the void ratio (Oda, et al, 1972c). If the three-dimensional distribution of N_i shows axial symmetry having a axis of symmetry parallel to Z-axis, $E(\alpha, \beta)$ can be regarded to be independent of α, and $E(\alpha, \beta)$ can be replaced by $E(\beta)$.

The techniques to measure the fabric components quantitatively and their influences on mechanical properties of granular material have already been discussed in the previous papers (Oda, 1972b and 1972c). The microscopic fabric of the deformed and undeformed specimens shown in Fig. 1 was analysed with the following results:

Void Ratio and its Variation within the Deformed and Undeformed Specimens

Results as shown in Figs. 2 to 4 clearly demonstrate that the distribution of void ratio within the specimens deformed beyond peak stress state are not uniform, although the undeformed and slightly deformed specimens are nearly uniform in regard to void ratio. The central parts of the specimens which are deformed above peak stress state show an extraordinarily large void ratio ranging from 0.80 to 0.87 for specimens of P- and T-series

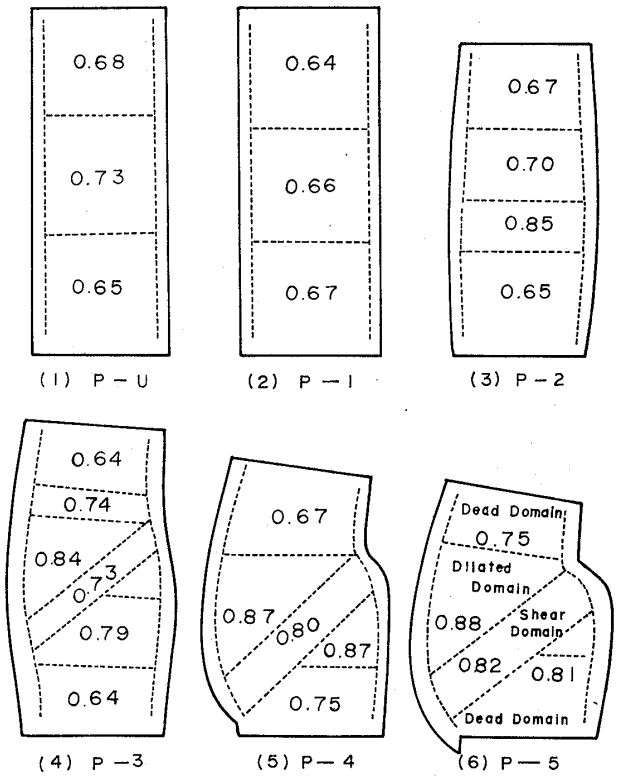

Fig. 2. Void ratios and their variation within specimens (P-series experiments)

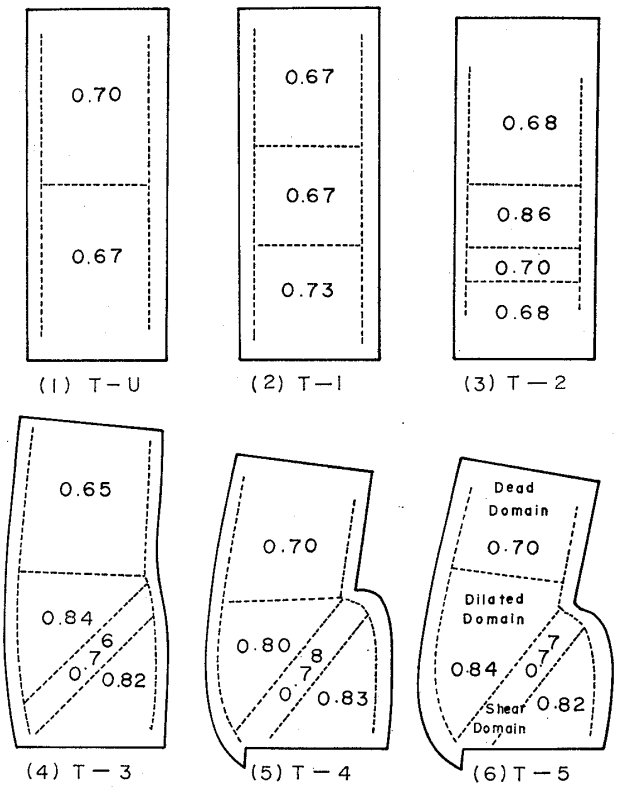

Fig. 3. Void ratios and their variation within specimens (T-series experiments)

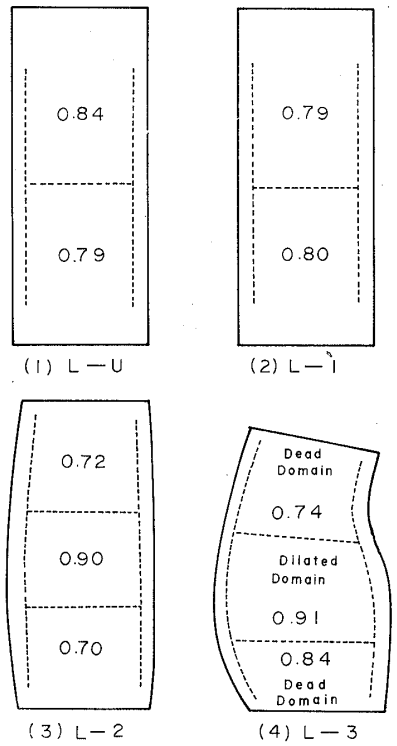

Fig. 4. Void ratios and their variation within specimens (L-series experiments)

Table 2. Results of drained triaxial tests

Series of experiments	Name of specimens	Final axial strain (%)	Final axial stress ratio	Maximum stress ratio	Modulus of deformation (kg/cm²)	General trend of shear plane γ' (degree)
P-series	P-U	undeformed	1.00	——	——	——
	P-1	0.72	2.81	——	——	——
	P-2	10.88	3.87	3.96	340	——
	P-3	13.65	3.55	4.03	240	40
	P-4	23.81	3.10	4.01	210	42
	P-5	31.26	2.76	3.95	250	43
T-series	T-U	undeformed	1.00	——	——	——
	T-1	0.64	3.26	——	——	——
	T-2	3.97	4.34	4.34	310	——
	T-3	9.28	3.67	4.44	280	55
	T-4	20.00	2.91	4.43	440	58
	T-5	22.54	2.93	4.18	260	60
L-series	L-U	undeformed	1.00	——	——	——
	L-1	2.38	2.97	——	——	——
	L-2	11.90	3.49	3.51	140	——
	L-3	24.00	2.81	3.41	140	——

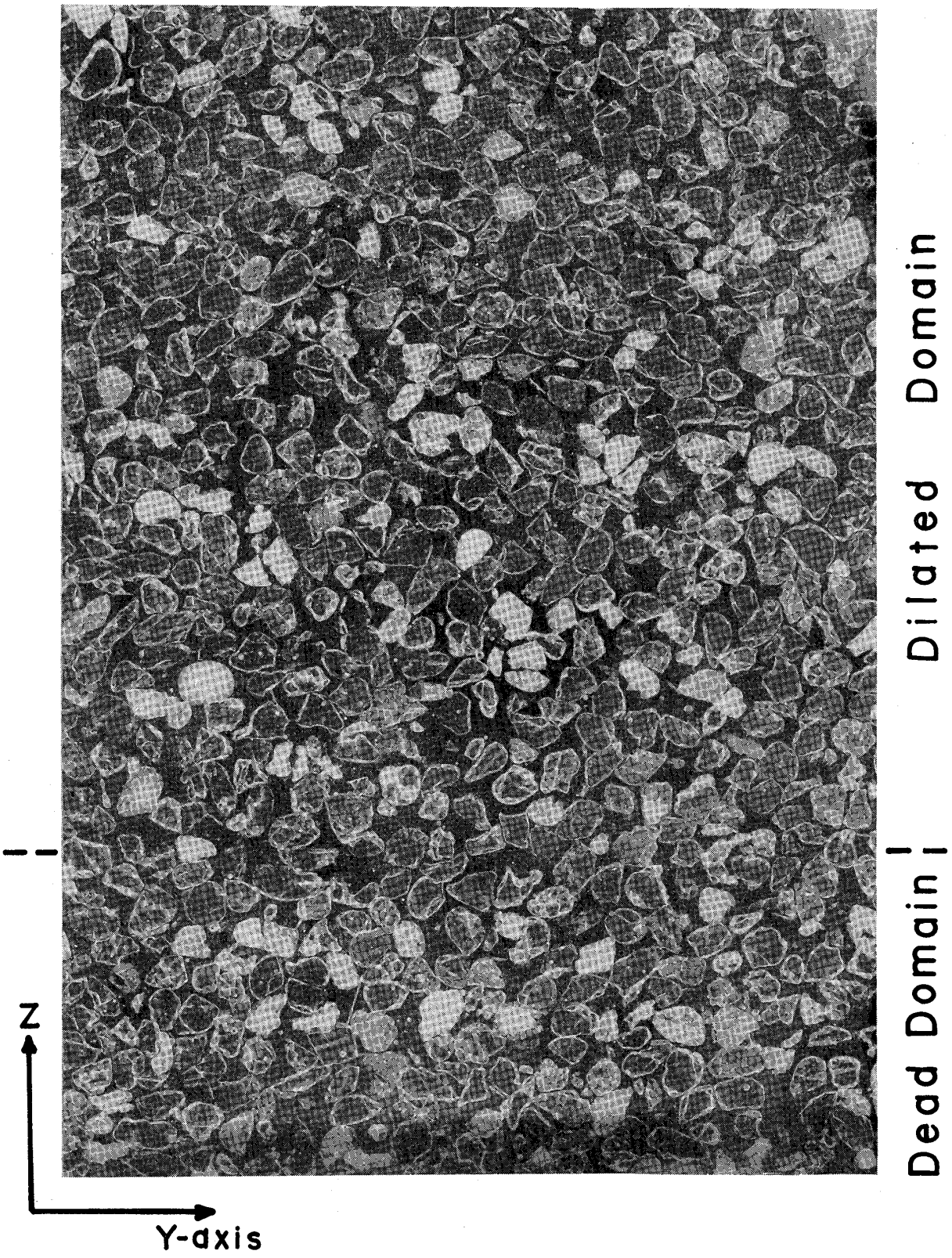

Photo. 1. Photograph showing the dead and dilated domains

experiments and from 0.90 to 0.91 for specimens of L-series experiments. This domain, which will be called "dilated domain" henceforth, has a larger void ratio than other parts of the same specimen. The void ratio of the dilated domain is almost equivalent to 20% relative density. It is concluded that volume expansion due to dilatancy occurred mostly at a narrow central domain until the peak stress state (cf. Roscoe, 1963; Rowe, 1964), because little fluctuation with respect to the void ratio during deformation can be observed in other parts of test specimens.

In regard to the distribution of void ratio, the specimens deformed to the residual stress state can be divided into the following three statistically homogeneous domains:

(1) Dead domain (Photo 1): The formation of this domain at the end of specimens is due to the restraining effect of radial friction forces at the end plates, by which little fabric reconstruction occurred during deformation.

(2) Dilated domain (Photo 1): This domain is characterized by extraordinarily large void ratio. In the specimen deformed to peak stress state, the extent of this domain is circumscribed within narrow bonds (being one-sixth of the specimen). However, with increase of axial strain to the residual stress state, the domain continuously expands and the extent of dead domain at the end of specimen becomes narrow. Consequently the final volumetric strain in a drained compression test must be determined not only by the peculiar void ratio in the dilated domain but by the extent of final expansion of its domain.

(3) Shear domain (Photo 2): This domain also has large void ratio. It is worthy of attention that the void ratios in the shear domain which range from 0.73 to 0.82 are smaller than those in the dilated domain.

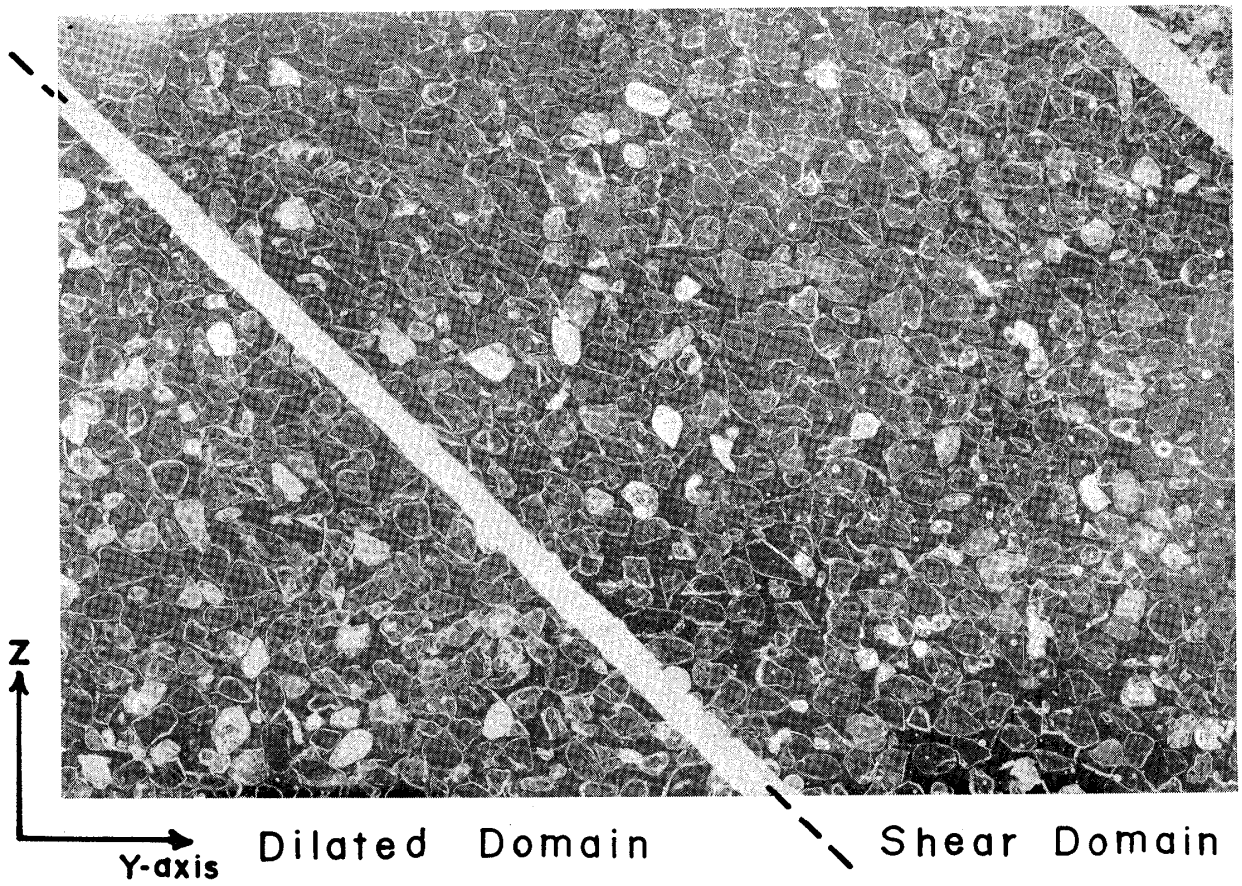

Photo. 2. Photograph showing the dilated and shear domains

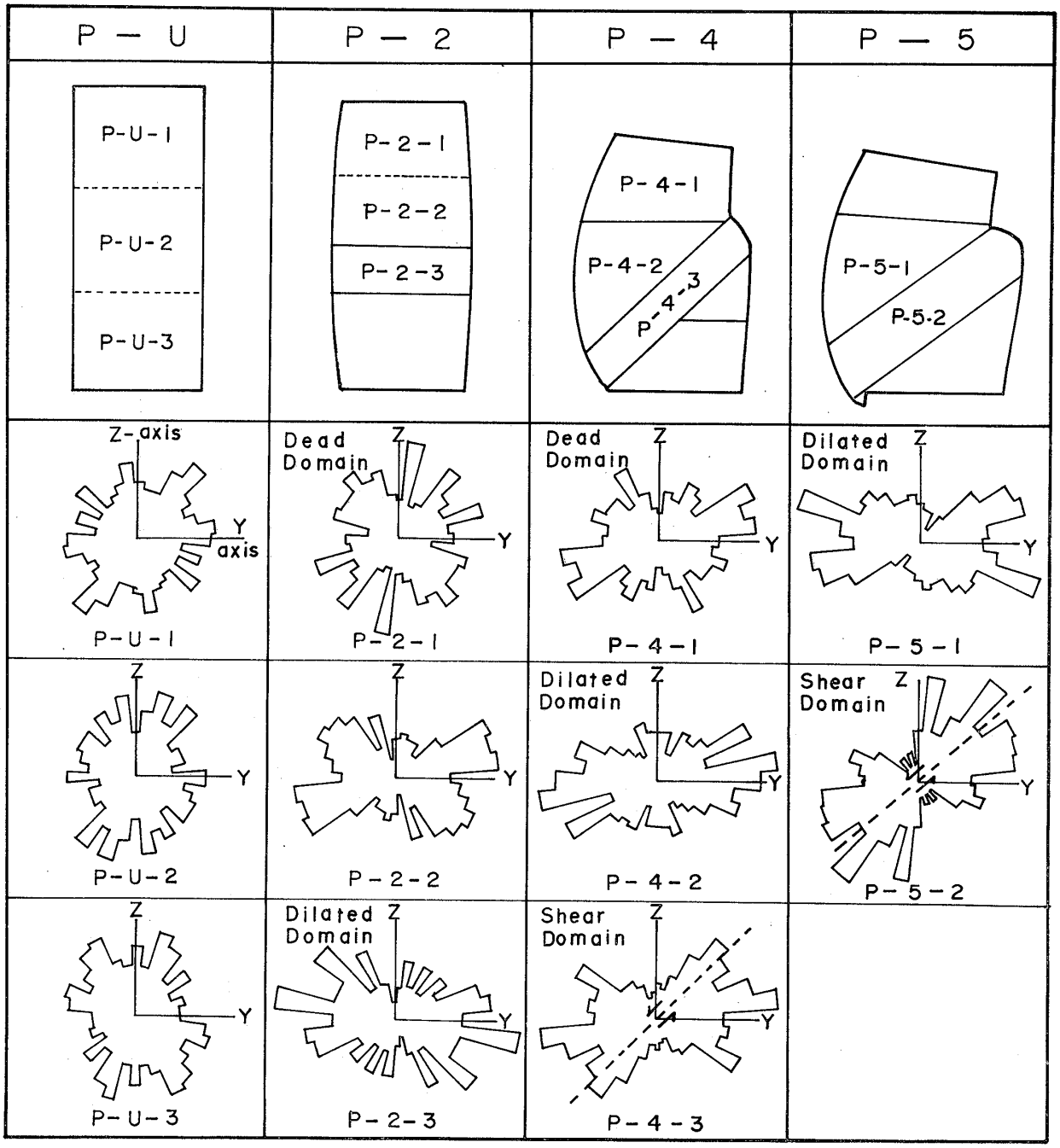

Fig. 5. Apparent dimensional orientation of grains in the V-section of specimens compacted by the plunging method

Reconstruction of Orientation Fabric during Deformation

Fig. 5 shows rose diagrams prepared from azimuths of apparent grain elongation measured in the V-sections of deformed and undeformed specimens (P-U, P-2, P-4 and P-5).

The strong concentration at 90° to the cylinder axis Z becomes conspicuous at the dilated domain as shown in P-2-3, P-4-2 and P-5-1. This fact reflects the tendency for the maximum projection area containing long and intermediate dimension of particle to rearrange near circular section of the specimen throughout deformation mechanism constructing the dilated domain. The rose diagrams for the dead domain of P-2 and P-4 specimens are almost the

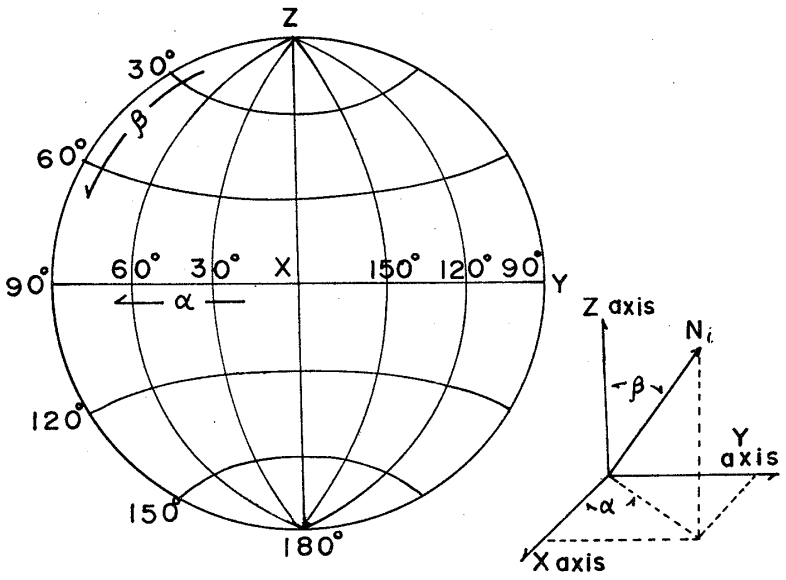

Fig. 6. Equal area net showing the reference axis and the angles α and β

same as those for the undeformed specimen (P-U). The preferred direction of apparent dimensional orientation shown by the rose diagrams for the shear domains (P-4-3 and P-5-2) changes progressively toward parallel to the general trend of shear domain which inclines to major principal plane at γ'. It must be noticed, however, that the preferred direction of dimensional orientation does not always coincide with the general trend of shear domain.

From the facts described above, it can be said that the rolling of grain particle must be a factor to control the mechanism of fabric reconstruction during the progressive deformation up to the residual stress state (Borg, et al., 1960; Oda, 1972b).

Change of the Function $E(\alpha, \beta)$ with Increasing Deformation

To show the three dimensional distribution of N_i in each homogeneous domain, the values of angles α and β measured at the contacts selected at random from two V-sections and one H-section (Oda, 1972a) are plotted on a lower equal area net in which the reference axes (X, Y and Z) are situated as shown in Fig. 6 (Turner and Weise, 1963; Friedman, 1964). The number of points falling within each one percent area is recorded as a percentage of the total number of points. The contour lines are drawn to emphasize the orientation pattern of N_i (Figs. 7 to 12).

The N_i -distribution of undeformed specimen compacted by the plunging method does not show any reproducible local concentration (Fig. 7). Comparing Fig. 7 with Figs. 8 and 9, it is clear that the normals at the contacts in the dilated domain gradually become to concentrate within small area of the ranges $0° \leq \beta \leq 50°$ and $130° \leq \beta \leq 180°$ during the deformation to peak stress state. It is worthy of note that fabric diagrams as shown by Figs. 8 and 9 show axial symmetry with the symmetry axis parallel to the cylindrical axis of specimen. On the other hand, the N_i-distribution of the dead domain of P-3 specimen (Fig. 10) shows almost the same characters as that of undeformed specimen (Fig. 7).

After the peak stress ratio $\left(\frac{\sigma_1}{\sigma_3}\right)_f$ has passed, the fabric anisotropy due to the concentration of the normals to Z-axis reduces even in the dilated domain (compare Fig. 11 with Fig. 9).

The distribution of N_i shows a reproducible local concentration whose central direction is inclined to Z-axis at 35° (Fig. 12). It must be noted that the direction of shear plane

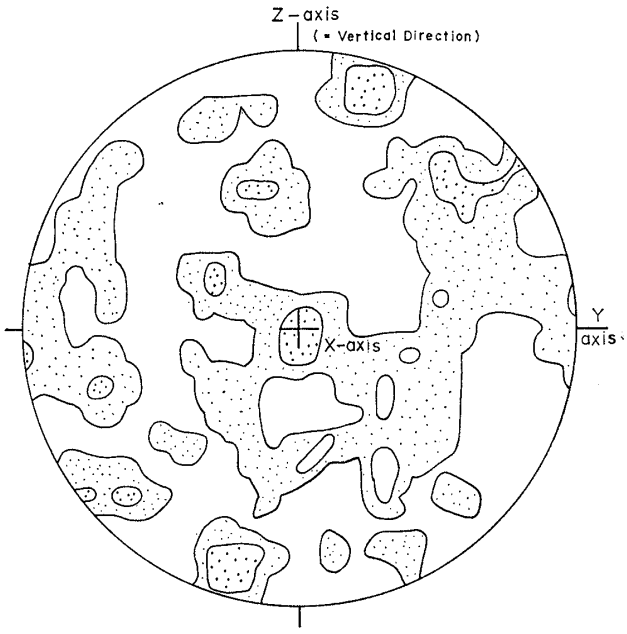

Fig. 7. Fabric diagram showing the Ni-distribution of P-U specimen (233 measurements; contour levels: 2% and 1% per 1% area)

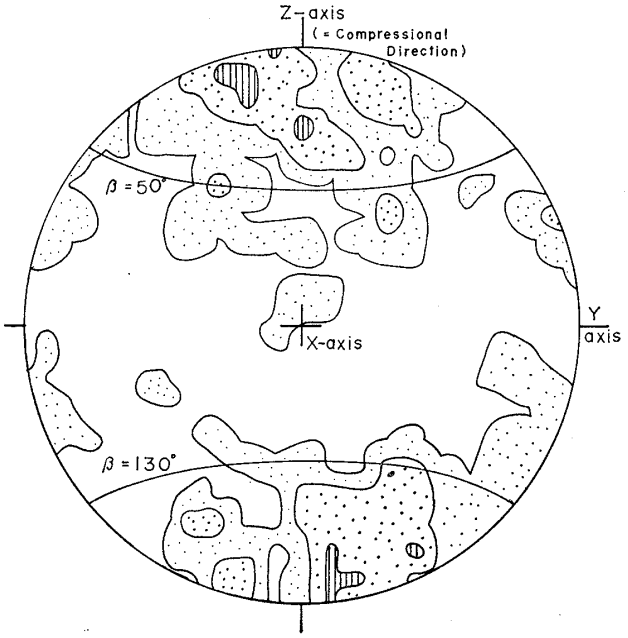

Fig. 8. Fabric diagram showing Ni-distribution of P-1 specimen (228 measurements; contour levels: 3%, 2% and 1% per 1% area)

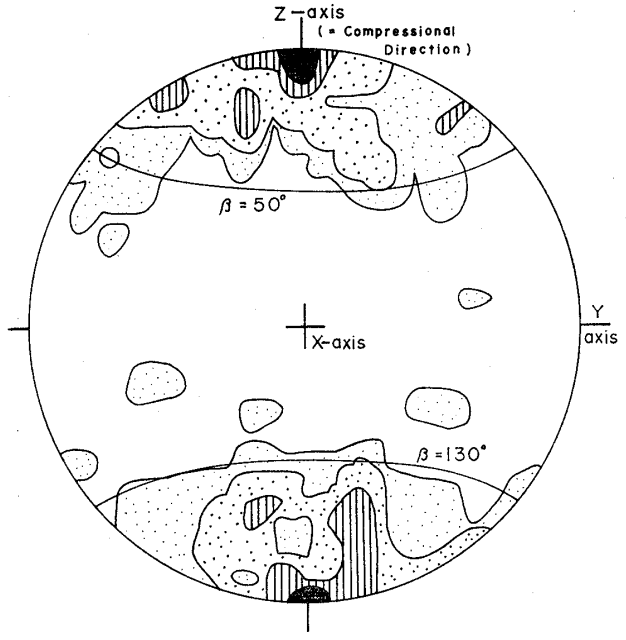

Fig. 9. Fabric diagram showing Ni-distribution of dilated domain of P-2 specimen (239 measurements; contour levels: 4%, 3%, 2% and 1% per 1% area)

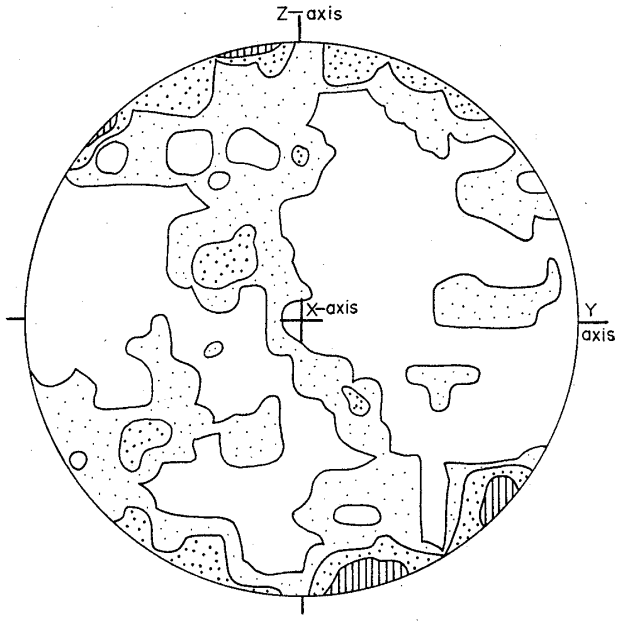

Fig. 10. Fabric diagram showing Ni-distribution of dead domain of P-2 specimen (181 measurements; contour levels: 3%, 2% and 1% per 1% area)

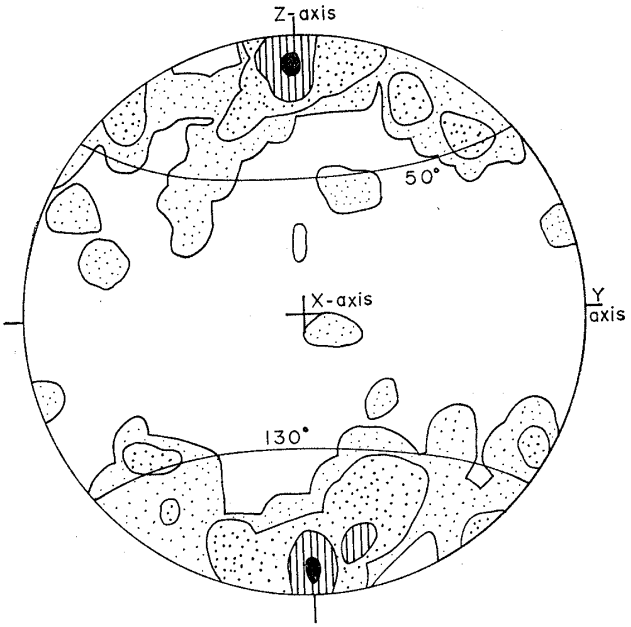

Fig. 11. Fabric diagram showing Ni-distribution of dilated domain of P-4 specimen (208 measurements; contour levels: 4%, 3%, 2% and 1% per 1% area)

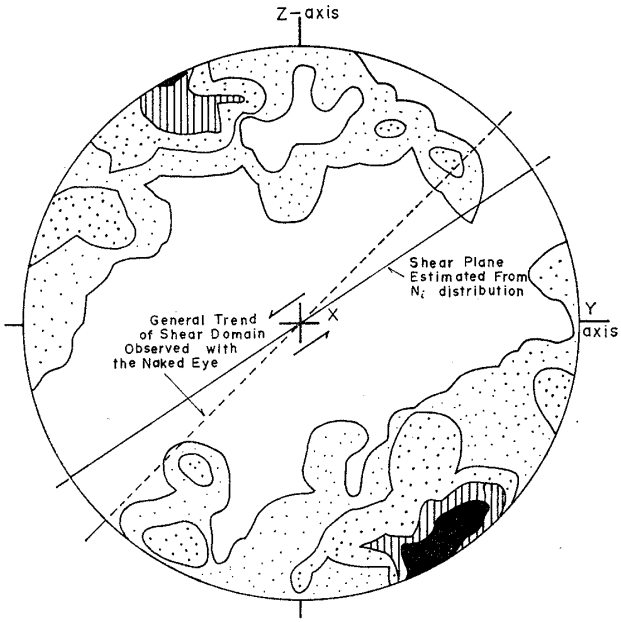

Fig. 12. Fabric diagram showing Ni-distribution of shear domain of P-5 specimen (165 measurements; contour levels: 4, 3, 2 and 1% per 1% area)

estimated from N_i-distribution of shear domain does not coincide with the general trend of shear domain observed in the deformed specimen with the unaided eyes.

MICROSCOPIC MECHANISM OF DEFORMATION

Based on the facts described in the previous sections it is reasonable to divide the stress-strain curve into three stages, i.e., strain hardening stage, transitional stage, and steady state stage (Fig. 13), to discuss each mechanism of deformation.

Microscopic Mechanism of Deformation in the Strain Hardening Stage

The fabric reconstruction in this stage is characterized by the concentration of N_i to the maximum principal stress direction (Z-axis). The contacts whose normals are parallel to σ_1-direction must be most effective in supporting the axial load, and the ability to support axial load at a contact may generally decreases with the increase of the angle (β) between σ_1-direction and the normal at the contact. Consequently it is natural to consider that the concentration of normals must play an essential role in hardening a granular material during compressional deformation to peak stress state (mechanism of strain hardening).

At an early part of this stage, the process of strain hardening may be accompanied with collapse of weaker parts of granular mass and the granular fabric of sand must become homogeneous throughout the specimen. At this early stage, the volumetric strain is compressional. At a latter part of this stage, however, the frictional resistance of grains is overcome and the granular particles move to dilate (cf., Kirkpatrick, 1957), and the normals to the contacts are concentrated to the maximum principal stress direction. Thus the initial fabric is wholly reconstructed and the homogeneity of granular fabric is lost.

If we assume that deformation of microscopic scale occurs as relative sliding between rigid particles without rolling at contacts, the resultant forces resolved in the X, Y and Z

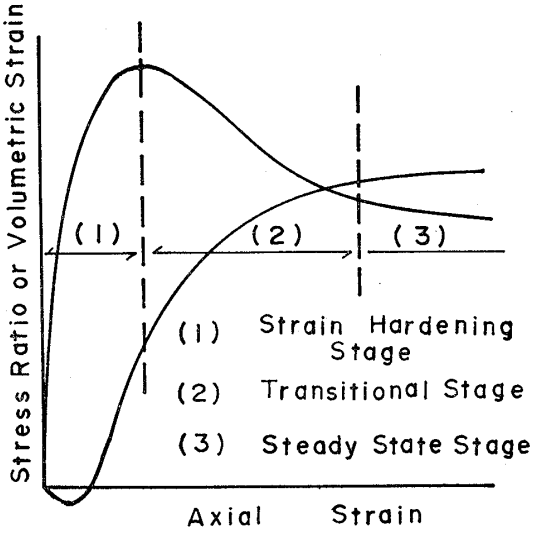

Fig. 13. Division of stress-strain curve into three stages

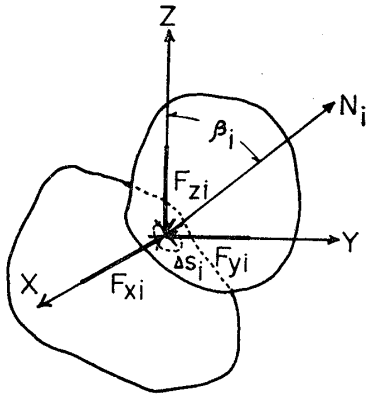

Fig. 14. Resultant forces resolved in the principal directions

directions (or principal stress directions) meet at a contact C_i (Fig. 14). The value of F_{zi} may be variable through the contacts within granular mass. However, the mean value ($\bar{F}_{zi}$) of the random variable (F_{zi}) can be considered to be a function of β_i, that is,

$$\bar{F}_{zi}=g(\beta_i)=g(\pi-\beta_i) \tag{1}$$

where $0\leq\beta_i\leq\frac{1}{2}\pi$.

Since the ability to support the axial load decreases with the increase of β_i, the value of the function $g(\beta_i)$ takes a maximum value when $\beta_i=0$ and a minimum value when $\beta_i=\frac{1}{2}\pi$. The function $g(\beta_i)$ can be determined as a function of β_i by assuming that $\bar{F}_{zi}$ at the contact C_i should be proportional to the area of the contact surface projected on the horizontal plane (X-Y plane).

$$\bar{F}_{zi}=g(\beta_i)=k_z\,\Delta S_i\cos\beta_i \tag{2}$$

From the same considerations with respect to X and Y directions, the following equations are obtained;

$$\left.\begin{aligned}\bar{F}_{xi}&=k_x\,\Delta S_i|\cos\alpha_i|\cdot\sin\beta_i\\ \bar{F}_{yi}&=k_y\,\Delta S_i|\sin\alpha_i|\cdot\sin\beta_j\end{aligned}\right\} \tag{3}$$

where $0\leq\alpha_i\leq2\pi$, $0\leq\beta_i\leq\frac{\pi}{2}$, ΔS_i=the area of contact surface at the contact C_i, and k_x, k_y and k_z=coefficients whose values must be determined by the condition of mobilized principal stress state as well as by the fabric characters of granular material.

Now, let us consider a unit cube having a dimension $L\times L\times L$ as shown in Fig. 15. The centroids of grains G_1, $G_2\cdots G_{nz}$ are situated within the unit cube. Consider these grains contact with the grains G_1', $G_2'\cdots G'_{nz}$ of the outside of the unit cube at the contacts C_1, $C_2\cdots C_{nz}$. The normals at these contacts are represented by N_1, $N_2\cdots N_{nz}$, respectively.

The summation of the axial forces transmitted by the contacts C_1, C_2 $\cdots$, C_{nz} in the compressional direction must be equal to $\sigma_1 \times L^2$ if the number of contacts (n_z) are sufficiently large. Then we get

$$\sigma_1 \times L^2 = \sum_{i=1}^{nz} \bar{F}_{zi} = k_z \sum_{i=1}^{nz} \Delta S_i \cdot \cos \beta_i = n_z k_z \overline{\Delta S} \cdot \overline{\cos \beta_i} \qquad (4)$$

where $\overline{\Delta S}$ and $\overline{\cos \beta_i}$ are the mean values of ΔS_i and $\cos \beta_i$ respectively. When we introduce the function $E(\alpha, \beta)$ representing the three-dimensional probability density of N_i, $\overline{\cos \beta_i}$ is calculated by the following equation;

$$\overline{\cos \beta_i} = \int_0^{\pi/2} \int_0^{2\pi} E(\alpha \cdot \beta) \sin 2\beta \, d\alpha \, d\beta \qquad (5)$$

where $\int_0^{\pi} \int_0^{2\pi} E(\alpha, \beta) \sin \beta \, d\alpha \, d\beta = 1$ and $E(\alpha, \beta) = E(\pi + \alpha, \pi - \beta)$.

Thereupon the coefficient k_z is determined by putting Eq. (5) into Eq. (4) as follows;

$$k_z = \frac{\sigma_1 \cdot L^2}{\overline{\Delta S} \cdot n_z \cdot \int_0^{\pi/2} \int_0^{2\pi} E(\alpha, \beta) \sin 2\beta \, d\alpha \, d\beta} \qquad (6).$$

With the same considerations with respect to X and Y directions, the constants k_x and k_y are determined in the case of the stress state of $\sigma_1 > \sigma_2 = \sigma_3$.

$$\left.\begin{aligned} k_x &= \frac{\sigma_3 \cdot L^2}{\overline{\Delta S} \cdot n_x \cdot \int_0^{\pi} \int_{-\pi/2}^{\pi/2} 2E(\alpha, \beta) \cos\alpha \sin^2\beta \, d\alpha \, d\beta} \\ k_y &= \frac{\sigma_3 \cdot L^2}{\overline{\Delta S} \cdot n_y \cdot \int_0^{\pi} \int_0^{\pi} 2E(\alpha, \beta) \sin \alpha \sin^2\beta \, d\alpha \, d\beta} \end{aligned}\right\} \qquad (7).$$

As we consider only about homogeneous fabric of granular material, $n_x = n_y = n_z = n$.

Now, let us consider static equilibrium of the resultant forces resolved in the principal stress directions at the contact C_i (Fig. 16). As the relative movements between particles were assumed to be due to sliding rather than due to rolling, the forces meet at a center of contact and sliding occurs along intersection of the plane containing both of directions N_i and Z and the tangential plane at sliding contact (Horne, 1969). The reference axes X and Y can be selected at our option in the horizontal plane when both of stress state and granular fabric show axial symmetry having the common axis of symmetry parallel to the vertical direction (Z). The X-axis is then selected in the plane containing both of directions N_i and Z (Fig. 16). Then the mean value of forces $\bar{F}_{xi}$, $\bar{F}_{yi}$ and $\bar{F}_{zi}$ are given by inserting $\alpha_i = 0$ into Eqs. (2) and (3),

$$\left.\begin{aligned} \bar{F}_{xi} &= k_x \cdot \Delta S_i \cdot \sin \beta_i \\ \bar{F}_{yi} &= k_y \cdot \Delta S_i \cdot 0 \\ \bar{F}_{zi} &= k_z \cdot \Delta S_i \cdot \cos \beta_i \end{aligned}\right\} \qquad (8).$$

As the ratio of tangential to normal force at contacts can not exceed the interparticle friction angle (ϕ_μ), interparticle sliding will occur at the contact C_i if the following equality is satisfied;

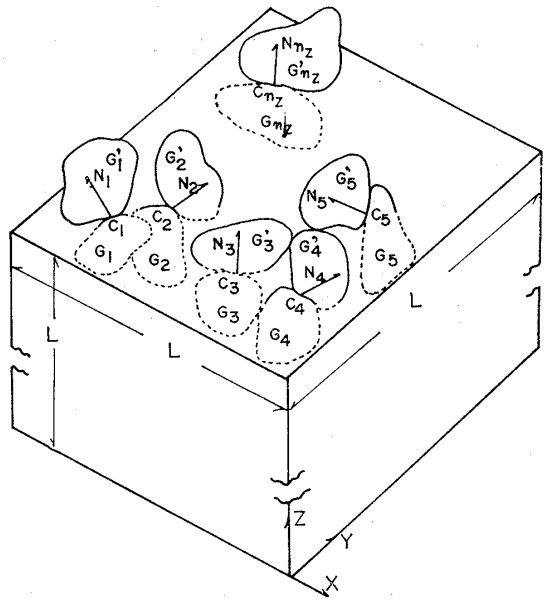

Fig. 15. A unit cube containing constituting grain particles

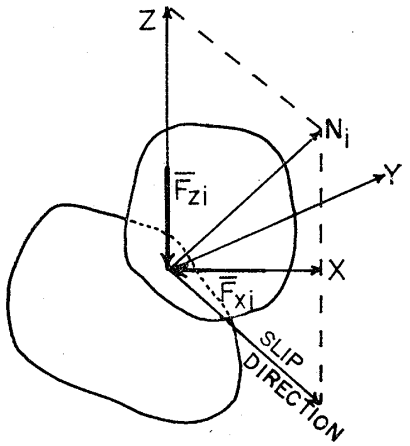

Fig. 16. Instantaneous interparticle slip

$$\frac{\bar{F}_{zi}}{\bar{F}_{xi}} = \tan\left(\frac{\pi}{2} + \phi_\mu - \beta_i\right) \tag{9}$$

Putting Eqs. (7) and (8) into Eq. (9), we get

$$\frac{\sigma_1}{\sigma_3} = \frac{\Delta S \cdot n \int_0^{\pi/2}\int_0^{2\pi} E(\alpha, \beta) \sin 2\beta \, d\alpha \, d\beta}{\Delta S \cdot n \int_0^{\pi}\int_{-\pi/2}^{\pi/2} 2E(\alpha, \beta) \cos\alpha \sin^2\beta \, d\alpha \, d\beta} \cdot \tan\beta_i \cdot \tan\left(\frac{\pi}{2} + \phi_\mu - \beta_i\right) \tag{10}$$

If we use the fabric index of granular materials (S_z/S_x) which has been introduced previously by the present writer (Oda, 1972b), Eq. (10) can be rewritten simply as follows;

$$\frac{\sigma_1}{\sigma_3} = \frac{S_z}{S_x} \tan\beta_i \cdot \tan\left(\frac{\pi}{2} + \phi_\mu - \beta_i\right) \tag{11}$$

Differentiating the right side of Eq. (11) with respect to β_i, the value of stress ratio is found to have minimum value when

$$\beta_c = \frac{\pi}{4} + \frac{1}{2}\phi_\mu \tag{12}$$

When inserting this value into Eq. (11), we get

$$\frac{\sigma_1}{\sigma_3} = \frac{S_z}{S_x} \tan^2\left(\frac{\pi}{4} + \frac{1}{2}\phi_\mu\right) \tag{13}$$

Rowe (1962) showed that ϕ_μ for quartz in water varies from 31° for silt to 22° for pebbles in the pressure range of 2 to 100 lb./in^2. Inserting these values into Eq. (13) results in the theoretical lines in Fig. 17. The symbols in Fig. 17 are obtained from experimental results of sands. Fig. 17 indicates that experimental results are well in accord with the theoretical lines throughout early stage of deformation to failure irrespective of their initial void ratio and initial fabric, even though the writer neglects the rolling of constituting grains.

Rowe (1962, 1963) demonstrated that microscopic slidings among constituting grains

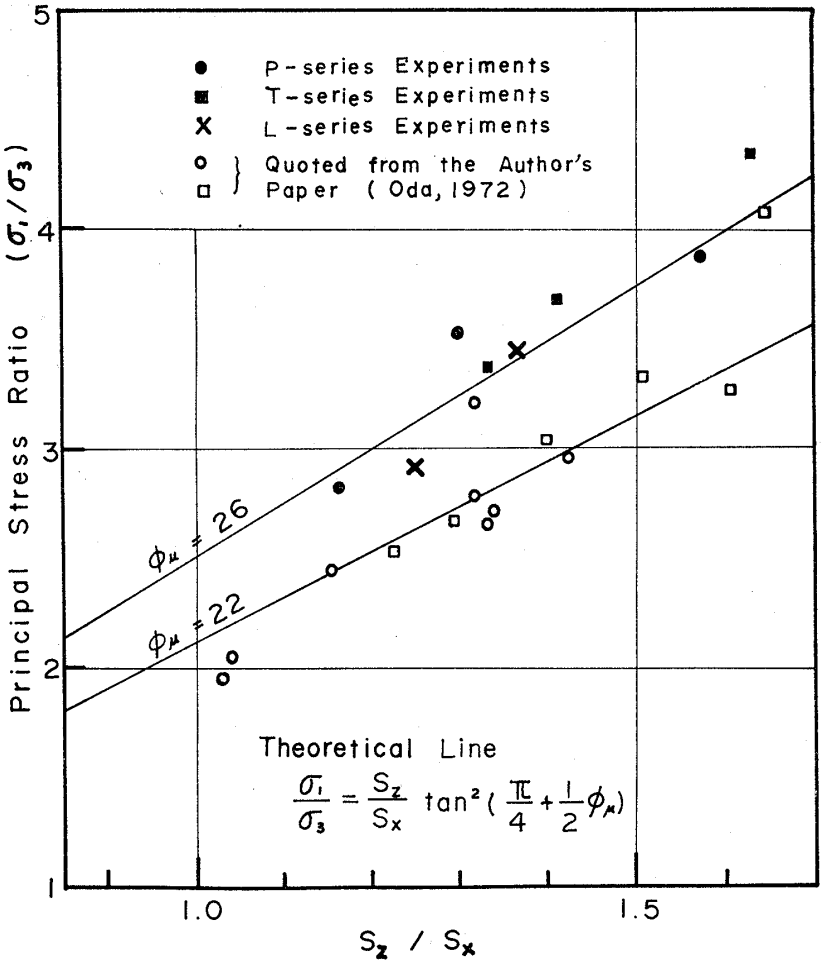

Fig. 17. Relation between stress ratio $\left(\frac{\sigma_1}{\sigma_3}\right)$ and fabric anisotropy $\left(\frac{S_z}{S_x}\right)$

must occur in the most economical way and this would be achieved for a given granular fabric if the individual value of β were such that the ratio of rate of dissipitation of energy in friction to the rate of supply of energy is a minimum. The minimization of the ratio with respect to β gave $\beta_c' = \frac{\pi}{4} + \frac{1}{2}\phi_\mu$. It is important to notice that β_c' is equal to β_c which was determined by differentiating the right side of Eq. (11) to obtain a minimum value of $\frac{\sigma_1}{\sigma_3}$.

Major Factor to Determine the Maximum Principal Stress Ratio Mobilized in Granular Materials

The maximum principal stress ratio in granular material at failure $\left(\frac{\sigma_1}{\sigma_3}\right)_f$ must be determined directly by the maximum value of $\left(\frac{S_z}{S_x}\right)_{\max}$ which could be accomplished in granular fabric during compressional deformation. As described in the previous section, the increase of the ratio $\frac{S_z}{S_x}$ during the latter stage of strain hardening is accompanied with the increase

of the void ratio at the dilated domain, and the fabric reconstruction of granular materials which is closely related to their bearing ability must be chiefly due to the fatal disturbance of preexisting grain fabric. Such disturbance will result in a decrease of mechanical stability of granular fabric.

Bjerrum et al. (1961) have carried out triaxial compression tests on drained and undrained specimens with the greatest circumspection to tests of very loose sand. Fig. 18 shows the relation between the internal friction angle corresponding to maximum stress ratio and the average relative density at failure. The internal friction angle is found to decrease rapidly as the relative density decreased below 20%, resulting in a sharp bend of the curve at R_c. Thus the friction angles of very loose specimens are as low as about 15°.

Relative density of the dilated domain at peak stress state ranges between 15 and 30% which is almost identical to a peculiar relative density observed in Fig. 18. Consequently, it seems reasonable to assume that there is a critical value of relative density representing an unstable arrangement of particle configuration in compressional deformation. Strain hardening due to the concentration of N_i toward σ_1-direction must cease when the relative density of deformed granular material becomes close to the critical value.

Deformation Mechanism in the Transitional Stage

The fabric in the dilated domain of the specimen deformed up to this stage is considered to be stable to withstand the increasing stress ratio while the direction of maximum principal stress coincides exactly with the vertical direction during deformation. Then the dilated domain expands upward and downward. If the direction of maximum principal stress deviates from the vertical direction from one cause or another, the fabric in the dilated domain can not withstand the increasing stress ratio and finally collapses.

Deformation Mechanism in the Steady State Stage

Because the greater part of applied strain is absorbed in the shear domain, the characteristics of the steady state stage such as flattening of curves in stress-axial strain and volumetric strain diagrams (Fig. 1) are considered to be determined by the arrangement of grain particle and microscopic deformation mechanism in this domain. The fabric in the shear domain is diagrammatically represented by Fig. 19-(1). The relative movements between grain particles must occur principally by preferred sliding along the contacts having the normals (N_i) inclined to the maximum principal stress direction by 35°.

The particle configuration relation and the deformation mechanism as shown in Fig. 19-(1) might be represented by a granular model as shown in Fig. 19-(2) where γ is a inclination angle of sliding plane to the maximum principal plane.

For the shear sliding between two solid bodies in contact, we obtain the following relation between γ and stress ratio mobilized at residual stress state $\left(\frac{\sigma_1}{\sigma_3}\right)_R$, assuming that the cohesion is zero;

$$\left(\frac{\sigma_1}{\sigma_3}\right)_R=\frac{\sin 2\gamma+(1-\cos 2\gamma)\cdot\tan\phi_\mu}{\sin 2\gamma-(1+\cos 2\gamma)\cdot\tan\phi_\mu} \tag{14}$$

Putting $\frac{1}{4}\pi+\frac{1}{2}\phi_\mu$ into γ, Eq. (14) can be rewritten as follows;

$$\phi_\mu=\sin^{-1}\frac{\left(\frac{\sigma_1}{\sigma_3}\right)_R-1}{\left(\frac{\sigma_1}{\sigma_3}\right)_R+1} \tag{15}$$

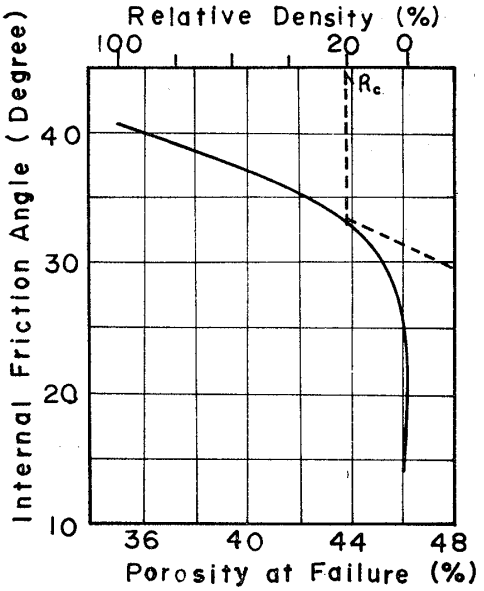

Fig. 18. Relation between internal friction angle and relative density at failure (Bjerrum, et al., 1961)

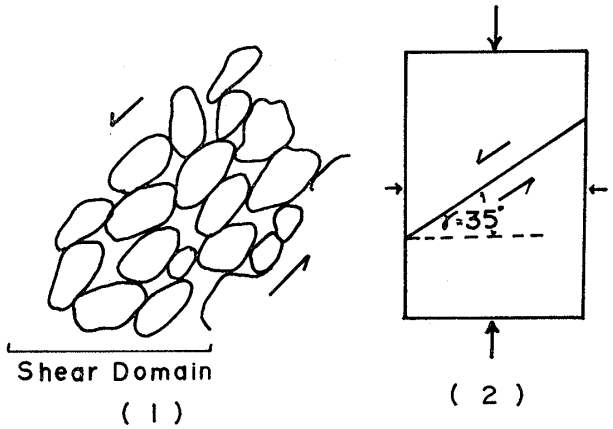

Fig. 19. Particle configuration relation and deformation mechanism in the shear domain

Eq. (15) shows that the internal friction angle calculated from a residual stress ratio must be equal to ϕ_μ when the employed granular model is accepted and γ is equal to $\frac{1}{4}\pi+\frac{1}{2}\phi_\mu$. The friction angle calculated from the right side of Eq. (15), however, does not coincide with ϕ_μ because generally the value of γ is not equal to $\frac{1}{4}\pi+\frac{1}{2}\phi_\mu$.

CONCLUSIONS

The present writer who tried to make clear the deformation mechanism of granular materials during deformation in triaxial compression obtained the following conclusions:

(1) The conspicuous characteristics of granular fabric in deformed specimens are their heterogeneity and anisotropy. The specimen of sand deformed to residual stress state can be divided into three subdomains having statistically homogeneous fabric with respect to void ratio, dimensional orientation of particles, and arrangement of normal directions to tangents, i.e., the dead domain, dilated domain and shear domain.

(2) A stress-strain curve can be divided into three stages on the basis of observations in regard to the mechanism of fabric reconstruction, i.e., the strain hardening stage, transitional stage, and steady state stage.

(3) The concentration of directions normal to tangents at contacts among constituting grains plays an essential role in hardening a granular material in the strain hardening stage.

(4) Mobilized stress ratio of granular material depends not only upon the interparticle friction angle ϕ_μ but also upon a parameter representing fabric anisotropy $\frac{S_z}{S_x}$.

(5) The dilated domain whose void ratio ranges from 15 to 30% relative density generally appears at the central narrow part of the specimen deformed to the peak stress state. Volume expansion due to dilatancy concentrates in this domain.

(6) The mechanical stability of granular materials is drastically reduced when its relative density becomes smaller than the critical relative density.

(7) In the shear domain, the inclination angle of major sliding direction of each grain particle to the direction of maximum principal stress is not equal to $\frac{1}{4}\pi + \frac{1}{2}\phi_\mu$. Generally, internal friction angle calculated from the stress ratio at residual stress state does not coincide with the interparticle friction angle of constituting grains.

ACKNOWLEDGEMENTS

The writer wishes to express his sincere gratitude to Prof. T. Onodera and Prof. Y. Seki of the University of Saitama for their kind advice throughout this work and also for critical reading of the manuscript. He is also indebted to Mr. H. Kobayashi and Mr. Y. Yamazaki for their support in performing this experimental work.

NOTATION

e_0=initial void ratio

$E(\alpha, \beta)$ or $E(\beta)$=three-dimensional probability density function of N_i

F_{xi}, F_{yi} and F_{zi}=resultant forces resolved in the principal stress directions at a contact C_i

$\overline{F}_{xi}$, $\overline{F}_{yi}$ and $\overline{F}_{zi}$=mean values of resultant forces F_{xi}, F_{yi} and F_{zi}

L=length of side of unit cube

n=number of contacts

N_i=directions perpendicular to tangential planes at contacts

ΔS_i=area of contact surface

$\overline{\Delta S}$=average area of contact surfaces

S_x, S_y and S_z=summations of projected area of each contact surface on the YZ-, ZX- and XY-planes

S_z/S_x=parameter representing fabric anisotropy

X, Y and Z=orthogonal reference axes

α and β=spherical coordinates to define the direction of N_i

γ=inclination angle of sliding plane to the maximum principal plane

σ_1=axial stress

σ_3=confining pressure

$(\sigma_1/\sigma_3)_R$=stress ratio mobilized at residual stress state

ϕ_μ=interparticle fricfion angle

REFERENCES

1) Bjerrum, L., Kringstad, S. and Kummeneje, O. (1961): "The shear strength of a fine sand," Proc. 5th Int. Conf. SMFE, Vol. 1, pp. 29-37.

2) Borg, I., Friedman, M., Handin, J. and Higgs, D. V. (1968): "Experimental deformation of St. Peter sand: A study of cataclastic flow," Rock Deformation, Geol. Soc. Am., Memoir 79, pp. 133-191.

3) Friedman, M. (1964): "Petrofabric techniques for the determination of principal stress directions in rocks," State of Stress in the Earth's Crust, American Elsevier Publishing Comp., pp. 451-552.

4) Horne, M. R. (1965): "The behaviour of an assembly of rotund, rigid, cohesionless particles, Parts 1 and 2," Proc. Roy. Soc. A., Vol. 286, pp. 62-97.

5) Horne, M. R. (1969): "The behaviour of an assembly of rotund, rigid, cohesionless particles, Part 3," Proc. Roy. Soc. A., Vol. 310, pp. 21-34.

6) Ingles, O. G. and Lee, L. K. (1971): "The influence of initial grain shape and pore anisotropy on strength of brittle soils," Geotechnique, Vol. 21, No. 2, pp. 143-153.
7) Kirkpatrick, W. M. (1957): "The condition of failure for sand," Proc. 4th Int. Conf. SMFE Vol. 1, pp. 172-178.
8) Lafeber, D. (1966): "Soil structural concepts," Engineering Geology, Vol. 1, No. 4, pp. 261-290.
9) Mogami, T. (1965): "A statistical theory of mechanics of granular materials," Jour. Fac. Engg., University of Tokyo (B), Vol. 28, pp. 65-79.
10) Mogami, T. (1966): "On the deformation on granular materials," Jour. Jap. Soc. Civ. Eng., No. 129, pp. 39-44.
11) Murayama, S. (1964): "Theoretical consideration on a behaviour of sands," Rheology and Soil Mechanics, Symposium, Grenoble, April 1-8, pp. 146-159.
12) Murayama, S. and Matsuoka, H. (1970): "A microscopic consideration on the shearing behaviour of granular materials using the two-dimensional models," Disaster Prevention Research Institute Annuals, No. 13, B, pp. 1-19. (in Japanese)
13) Newland, P. L. and Allely, B. H. (1957): "Volume changes in drained triaxial tests on granular materials," Geotechnique, Vol. 7, No. 1, pp. 17-34.
14) Oda, M. (1972a): "Initial fabrics and their relations to mechanical properties of granular material," Soils and Foundations, Vol. 12, No. 1, pp. 17-36.
15) Oda, M. (1972b): "The mechanism of fabric change during compressional deformation of sand," Soils and Foundations, Vol. 12, No. 2, pp. 1-18.
16) Oda, M., Kobayashi, H. and Yamazaki, Y. (1972c): "A new technique for determination of void ratio and its variation within deformed granular material," Report of Depart. Found. Engg., Faculty of Sci. and Engg., University of Saitama, Vol. 3, (in preparation).
17) Roscoe, K. H., Schofield, A. N. and Wroth, C. P. (1958): "On the yielding of soils," Geotechnique, Vol. 8, pp. 22-53.
18) Roscoe, K. H., Schofield, A. N. and Thurairajan, A. (1963): "An evaluation of test data for selecting a yield criterion for soils," Laboratory Shear Testing of Soils, ASTM, Special Technical Publication, No. 361, pp. 111-128.
19) Rowe, P. W. (1962): "The stress-dilatancy relation for static equilibrium of an assembly of particles in contact," Proc. Roy. Soc. A, Vol. 269, pp. 500-527.
20) Rowe, P. W. (1963): "Stress-dilatancy, earth pressure and slopes," Jour. Soil Mech. Found. Eng., Vol. 89, SM. 3, pp. 37-61.
21) Rowe, P. W. (1964): "Importance of free ends in triaxial testing," Jour. Soil Mech. Found. Eng., Vol. 90, SM. 1, pp. 1-27.
22) Rowe, P. W. (1964): "Discussion of conforth," Geotechnique, Vol. 14, No. 4, pp. 361-364.
23) Turner, F. J. and Weiss, L. E. (1963): Structural Analysis of Metamorphic Tectonites, McGraw-Hill Book Co., New York, pp. 194-255.
24) Wilkins, J. K. (1970): "A theory for the shear strength of rockfill," Rock Mechanics, Vol. 2, pp. 205-222.

(Received May 31, 1972)